Cell Metabolism
Article

Skeletal Muscle Is a Primary Target of SOD1^{G93A}-Mediated Toxicity

Gabriella Dobrowolny,[1] Michela Aucello,[1] Emanuele Rizzuto,[1] Sara Beccafico,[2] Cristina Mammucari,[3] Simona Bonconpagni,[2] Silvia Belia,[3] Francesca Wannenes,[4] Carmine Nicoletti,[1] Zaccaria Del Prete,[5] Nadia Rosenthal,[6] Mario Molinaro,[1] Feliciano Protasi,[2] Giorgio Fanò,[2] Marco Sandri,[7,8,9] and Antonio Musarò[1,10,*]
[1]Institute Pasteur Cenci-Bolognetti, Department of Histology and Medical Embryology, CE-BEMM and IIM, Sapienza University of Rome,Via A. Scarpa, 14 Rome 00161, Italy
[2]Ce.S.I. Centro Scienze dell'Invecchiamento, IIM, Università degli Studi G. d'Annunzio, Chieti 66100, Italy
[3]Laboratorio Interuniversitario di Miologia, Università di Perugia, 06100 Italy
[4]Department of Sciences of Human Movement and Sport, IUSM and INMM-CNR, Rome 00100, Italy
[5]Department of Mechanical Engineering, Sapienza University of Rome, Rome 00184, Italy
[6]EMBL Mouse Biology Program, Monterotondo 00016, Italy
[7]Dulbecco Telethon Institute, University of Padova
[8]Venetian Institute of Molecular Medicine
[9]Department of Biomedical Science
Padova 35100, Italy
[10]Edith Cowan University, Perth, Western Australia 6027, Australia
*Correspondence: antonio.musaro@uniroma1.it
DOI 10.1016/j.cmet.2008.09.002

SUMMARY

The antioxidant enzyme superoxide dismutase 1 (SOD1) is a critical player of the antioxidative defense whose activity is altered in several chronic diseases, including amyotrophic lateral sclerosis. However, how oxidative insult affects muscle homeostasis remains unclear. This study addresses the role of oxidative stress on muscle homeostasis and function by the generation of a transgenic mouse model expressing a mutant *SOD1* gene (*SOD1^{G93A}*) selectively in skeletal muscle. Transgenic mice developed progressive muscle atrophy, associated with a significant reduction in muscle strength, alterations in the contractile apparatus, and mitochondrial dysfunction. The analysis of molecular pathways associated with muscle atrophy revealed that accumulation of oxidative stress served as signaling molecules to initiate autophagy, one of the major intracellular degradation mechanisms. These data demonstrate that skeletal muscle is a primary target of SOD1^{G93A} -mediated toxicity and disclose the molecular mechanism whereby oxidative stress triggers muscle atrophy.

INTRODUCTION

The delicate balance between oxidant production and antioxidant defense is severely compromised in several pathological conditions, leading to muscle wasting (Moylan and Reid, 2007). The fact that mutation in the major antioxidant enzyme superoxide dismutase 1 (SOD1) is associated with one fifth of familial amyotrophic lateral sclerosis (ALS) has implicated oxidative stress as a key mechanism underlying the pathogenesis of this disease (Barber et al., 2006). ALS is an adult-onset disease that is characterized by the selective degeneration of motor neurons in the brain and spinal cord, resulting in progressive paralysis and death.

Although mutant *SOD1* is also expressed by muscle, it is not yet established whether its presence in skeletal muscle directly contributes to any pathological feature, including muscle atrophy and alteration in the functional performance. To date, alterations in ALS skeletal muscle have been considered the result of alterations in nerve activity and not the direct result of SOD1-mediated toxicity.

It has been reported that partial suppression of mutant SOD1 accumulation within muscle (50% decrease in *SOD1* mRNA and protein in the muscle fibers) (Miller et al., 2006) was not sufficient to delay the progression of the disease in the SOD1^{G93A} mouse, suggesting that residual mutant protein is sufficient to retain the pathological phenotype or that muscle is not a key component in pathogenesis of ALS.

To explore more directly whether skeletal muscle is a direct target of SOD1-mediated toxicity and to determine the specific contribution of oxidative stress to muscle atrophy and wasting, we generated transgenic mice in which the *SOD1* mutant gene (*SOD1^{G93A}*) was selectively expressed in skeletal muscle under the transcriptional control of muscle-specific promoter (MLC) (Grieshammer et al., 1992). This approach dissociates the alterations of skeletal muscle from motor neuron degeneration and allows definition of the intracellular signal perturbations activated by muscle-specific impairment of the antioxidant SOD1 enzyme. We show that muscle-restricted expression of the *SOD1^{G93A}* (*MLC/SOD1^{G93A}*) transgene was sufficient to induce severe muscle atrophy associated with significant reduction in muscle strength, sarcomere disorganization, significant changes in mitochondria morphology and disposition, and disorganization of the sarcotubular system. Analysis of signals activated by selective muscle accumulation of oxidative stress in *MLC/SOD1^{G93A}* transgenic mice revealed that along with the activation of FoxO

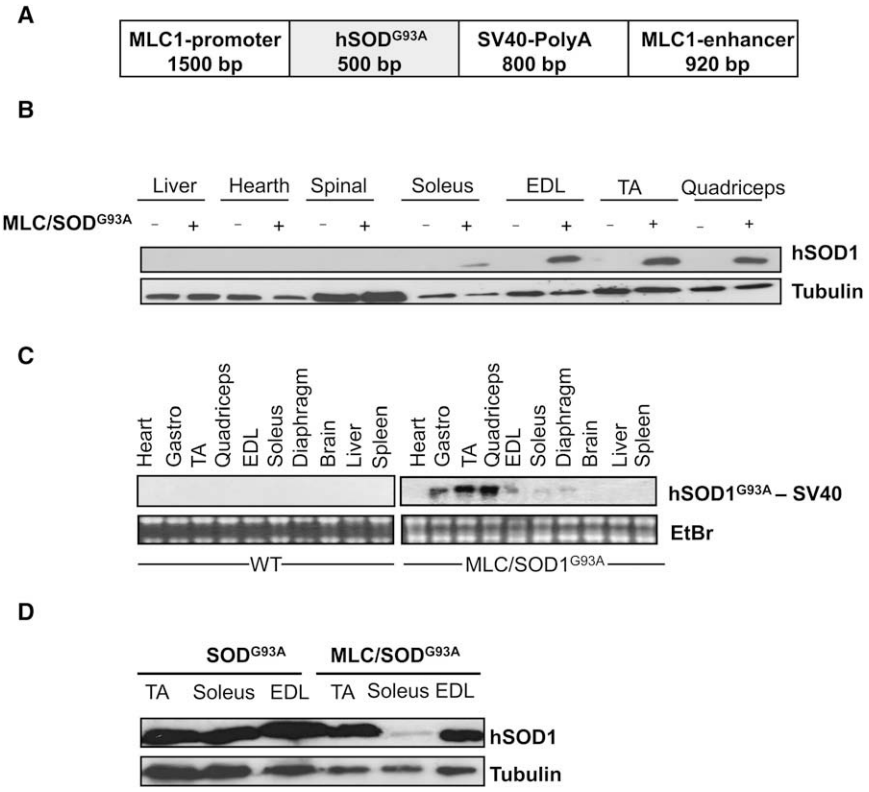

Figure 1. Characterization of MLC/SOD1^{G93A} Transgenic Mice

(A) Schematic representation of *MLC/SOD1^{G93A}* construct.

(B) Western blot analysis for human SOD1 protein in different tissues of both WT (–) and MLC/SOD1^{G93A} trangenic (+) mice.

(C) Northern blot analysis of total RNA samples (15 μg) from heart, brain, liver, spleen, and different skeletal muscles of both wild-type (WT) and transgenic mice was carried out with *PolyA SV40* 32P-labeled probe. Ethidium bromide staining was used to verify equal loading of the RNA. MLC/SOD1^{G93A} protein (B) and transcripts (C) are restricted to the fastest muscle types in transgenic mice and are undetectable in WT muscles.

(D) Western blot analysis for human SOD1 protein in TA, EDL, and soleus muscle of SOD1^{G93A} and MLC/SOD1^{G93A} mice.

and NFκB, both of which induce the expression of several atrophy-related genes, the accumulation of reactive oxygen species (ROS) served as signaling to initiate autophagy, one of the major intracellular degradation mechanisms that appears to be a key determinant for the induction of muscle atrophy. Ultrastructural analysis of *MLC/SOD1^{G93A}* muscle revealed the T-tubule as the potential donor of membrane that forms sequestering autophagocytic vesicles. The characterization of this mouse model and elucidation of the molecular mechanism that mediates muscle atrophy promises to significantly advance our understanding of the possible pathogenic mechanisms of oxidative stress that leads to muscle wasting in human diseases.

RESULTS

Selective Expression of Mutant *SOD1^{G93A}* Gene in Skeletal Muscle

To define the direct contribution of oxidative stress on muscle atrophy and wasting and verify whether skeletal muscle is a direct target of SOD1 mutation we generated transgenic mice with the mutated isoform of human superoxide dismutase 1 (*SOD1^{G93A}*) cDNA driven by skeletal muscle-specific regulatory elements from the rat myosin light chain (MLC)-1/3 locus (Grieshammer et al., 1992) (Figure 1A). Expression of the *MLC/SOD1^{G93A}* transgene in adult mice was restricted to skeletal muscle, predominated in muscles enriched in fast fibers, and reduced in slow muscles such as the soleus (Figures 1B and 1C), where the MLC regulatory cassette is characteristically expressed at very low levels (Grieshammer et al., 1992). Notably, no expression of human SOD1 protein and transcript were found in heart, brain, liver, spleen, or spinal cord (Figures 1B and 1C) of transgenic mice.

Western blot analysis (Figure 1D) also revealed that the levels of mutant SOD1 synthesis in tibialis anterior (TA) and extensor digitorum longus (EDL) muscles of MLC/SOD1^{G93A} adult mice were similar to the corresponding levels found in mice that develop ALS-like disease from ubiquitous expression of the same G93A mutant (Gurney et al., 1994). In contrast, soleus muscle of the classical SOD1^{G93A} mouse expressed higher levels of SOD1 mutant gene, compared to the corresponding muscle of MLC/SOD1^{G93A} mice (Figures 1B–1D), consistent with the fast fiber-selective pattern of endogenous MLC expression.

Muscle-Restricted Expression of SOD1^{G93A} Protein Causes Muscle Atrophy

To verify whether local accumulation of mutant SOD1 protein altered the muscle phenotype, we performed histological analysis on skeletal muscles of 10-day-old (neonatal), 4-week-old (young), and 16-week-old (adult) transgenic mice. While hematoxylin and eosin staining did not reveal significant differences in muscle mass between wild-type (WT) and transgenic mice at 10 days old (data not shown), skeletal muscle atrophy in MLC/SOD1^{G93A} mice was first detectable at 4 weeks (Figures 2A and 2B), increasing into adulthood (16 weeks), when the transgenic mice showed significant reduction in cross-sectional area (CSA) of TA, soleus, and EDL muscle fibers compared with their age-matched WT sibs (Figures 2C and 2D). Notably, the relatively lower expression levels of MLC/SOD1^{G93A} transgene in soleus muscle, compared to EDL and TA (Figures 1B and 1C), were still sufficient to induce muscle atrophy (Figure 2C), supporting the evidence that SOD1^{G93A} toxic properties are independent of the levels of SOD1 activity. The frequency distribution of CSA (Figures 2B and 2D) revealed a shift of the median values toward the small size of muscle fibers in all muscles analyzed. Of note, WT MLC/SOD1 overexpression did not induce evident signs of muscle atrophy and any morphological sign of disease (data not shown).

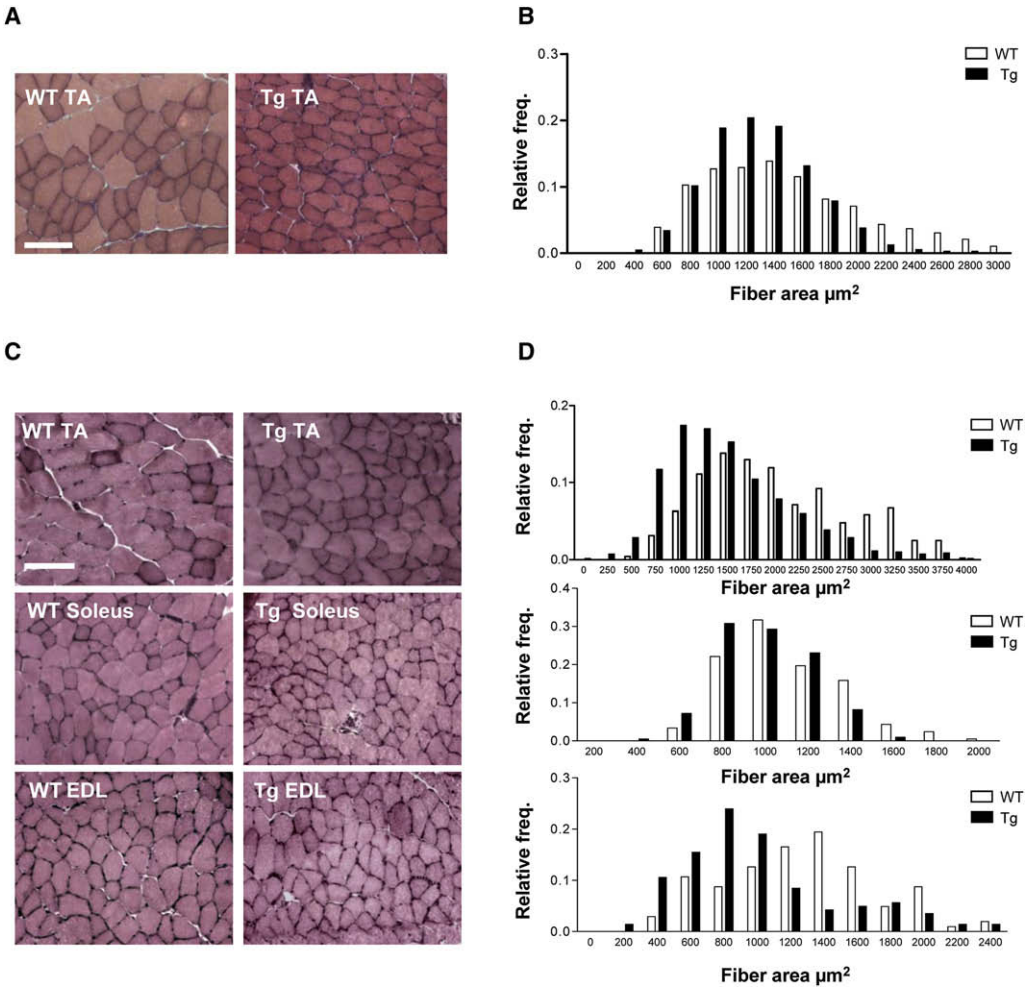

Figure 2. MLC/SOD1^{G93A} Expression Induces Severe Skeletal Muscle Atrophy

(A) Haematoxylin and eosin-stained cross-sections of tibialis anterior (TA) muscles from 1-month-old wild-type (WT) and MLC/SOD1^{G93A} transgenic (Tg) mice. Bar = 100 µm.

(B) Fiber size in WT (white bars) (n = 5) and MLC/SOD1^{G93A} transgenic (black bars) (n = 5) mice of TA muscles (mean ± SEM; TA WT = 1581.6 ± 22.2 µm^2; TA Tg = 1293.7 ± 10.7 µm^2. Mann-Whitney Rank Sum test: $p < 0.001$).

(C) Haematoxylin and eosin-stained cross-sections of TA, soleus, and EDL muscles from 4-month-old WT and MLC/SOD^{G93A} transgenic (Tg) mice. Bar = 100 µm.

(D) Fiber size in wild-type (white bars) (n = 5) and MLC/SOD1^{G93A} transgenic (black bars) (n = 5) mice of TA (upper panel), soleus (central panel), and EDL (lower panel) muscles (mean ± SEM; TA WT = 2073.3 ± 38.1 µm^2; TA Tg = 1503.8 ± 25.3 µm^2; Soleus WT = 1099.2 ± 18.9 µm^2; Soleus Tg = 991.6 ± 15.1 µm$^{2;}$; EDL WT = 1274.6 ± 44.5 µm^2; EDL Tg = 993.9 ± 40.3 µm^2. Mann-Whitney Rank Sum test: $p < 0.001$).

Mutant *SOD1* Alters the Functional Performance and the Contractile and Metabolic Machinery of Skeletal Muscle

To determine whether muscle accumulation of SOD1^{G93A} mutant protein affected the capacity to produce force, a direct comparison of mechanical parameters was performed for the soleus and EDL muscles of both WT and MLC/SOD1^{G93A} transgenic mice at 16 weeks of age. Muscle atrophy in transgenic mice was associated with decreased tetanic and specific force generation of 37% for EDL and 39% for soleus muscle compared with age-matched WT littermates (Figures 3A, 3B, 3D, and 3E). This trend was confirmed by the analysis of isotonic fatigue. In the first seconds of fatigue, stimulation of both transgenic EDL and soleus produced work of about 38% less than WT muscles (Figures 3C and 3F). Furthermore, MLC/SOD1^{G93A} EDL and soleus stopped shortening about 7 s and 15 s, respectively, before the WT controls. These analyses demonstrate that even low levels of mutant SOD1^{G93A} transgene expression, such as those in the soleus muscle, were sufficient to compromise the morphological and functional parameters of skeletal muscle.

The altered muscle phenotype of the MLC/SOD1^{G93A} mice was confirmed by ultrastructural analysis. In electron microscopy (EM), adult skeletal muscle fibers are characterized by a highly ordered organization of their major apparatii (Franzini-Armstrong, 1970): the contractile apparatus (the myofibrils), the excitation-contraction (EC) coupling units (formed by the sarcotubular system), and the metabolic machinery (the mitochondria), which are usually regularly shaped with a dark/dense internal matrix and specifically positioned between the Z lines and triads (Ogata and Yamasaki, 1985). Fibers in EDL muscles from MLC/SOD1^{G93A} transgenic mice showed clear alterations

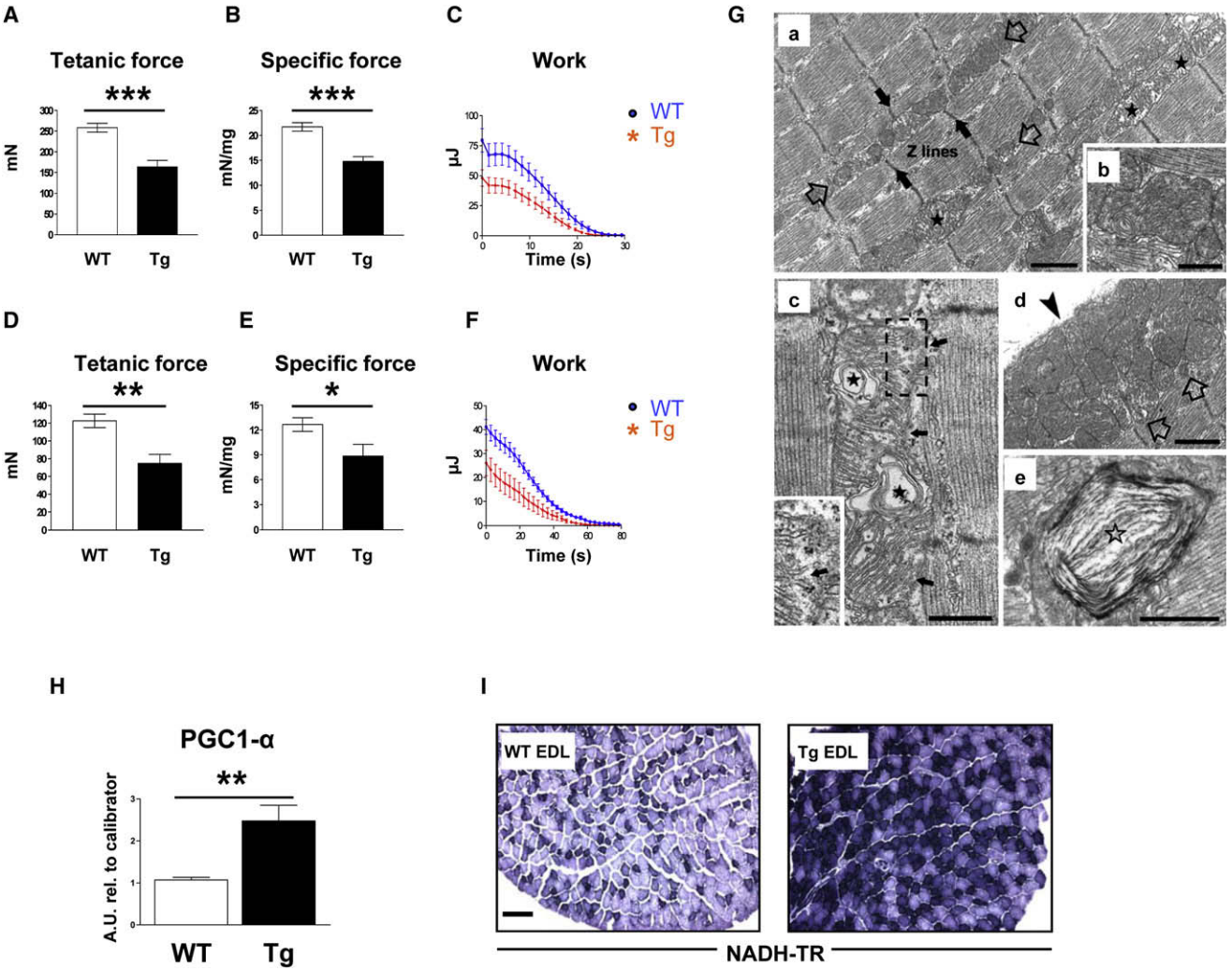

Figure 3. MLC/SOD1^{G93A} Expression Affects the Functional Performance of Skeletal Muscle

(A–F) Physiological properties of EDL and soleus muscles from 4-month-old WT and Tg mice. EDL (upper panels) and soleus muscles (lower panels) from wild-type (n = 10) and transgenic (n = 10) mice were compared by tetanic force (left), specific force (center), and work (right). All measurements are presented as mean ± SEM (*p = 0.022; **p = 0.0015; ***p < 0.0001).

(G) Electron microscopy of MLC/SOD1^{G93A} EDL muscles. In MLC/SOD1^{G93A} transgenic muscle, myofibrils were often out of register (panel a, black arrows), and mitochondria were clustered in longitudinal rows between the myofibrils (panel a, empty arrows). Mitochondria were swollen (panel a, stars), abnormally shaped, and larger in size (panel b, giant mitochondria). In several cases abnormal mitochondria contained vacuolization (panel c, stars), disrupted external membrane (panel c, dashed box and enlarged detail), and large myelin-like figures (panel e, empty star). Large clusters of mitochondria located just under the sarcolemma (panel d, large arrows) were more frequent in transgenic muscle (panel d, arrowhead). Bars: a and d, 1 μm; b, c, and e, 0.5 μm.

(H) Real-time PCR analysis of *PGC1α* transcript in both WT and MLC/SOD1^{G93A} transgenic (Tg) muscles (**p = 0.0093). Values are reported as mean ± SEM.

(I) NADH-TR staining of WT and MLC/SOD1^{G93A} (Tg) EDL muscles shows a shift from glycolitic to oxidative metabolism (darker fibers). Bar = 100 μm.

of their internal organization, including partial loss or misalignment of sarcomeres, significant changes of mitochondria morphology and of their sarcomeric disposition, and disorganization of the sarcotubular system (Figure 3G). In these fibers, Z lines of adjacent myofibrils tended to loose register with one another (Figure 3Ga, black arrows). Mitochondria were often clustered in abnormal longitudinal rows between the myofibrils and/or large clusters located just under the sarcolemma (Figure 3Ga and 3Gd, empty arrows). In addition, mitochondria were frequently abnormally shaped, were larger in size (Figure 3Gb, giant mitochondria), and presented a translucent appearance, edematous internal matrix with abnormal and/or missing internal cristae (Figure 3Gc, dashed box and enlarged detail), vacuolization (Figure 3Gc), and myelin-like figures (Figure 3Ge). Interestingly, similar alterations in myofibrillar structure and in mitochondria disposition have been described in aging skeletal muscle (Boncompagni et al., 2006 and data not shown) and in skeletal muscle biopsies of ALS patients (Chung and Suh, 2002).

The Peroxisome proliferator-activated receptor gamma coactivator 1α (PGC1α) is one of the major regulators of several crucial aspects of energy metabolism. PGC1α controls many aspects of oxidative metabolism (St-Pierre et al., 2006), including mitochondrial biogenesis (Lin et al., 2002), and it is the master regulatory gene that promotes fiber-type switching from

glycolytic toward more oxidative fibers (Lin et al., 2002). Real-time polymerase chain reaction (PCR) revealed that *PGC1α* expression was significantly increased in EDL muscle of MLC/SOD1^{G93A} transgenic mice (Figure 3H).

Notably, the accumulation of *PGC1α* was also associated with a shift in the metabolic activity of EDL muscle fibers to a more oxidative phenotype in MLC/SOD1^{G93A} transgenic mice, as shown by greater content of NADH (Figure 3I). Taken together these results demonstrate that oxidative stress significantly alters the metabolic activity of skeletal muscles.

Local Expression of *SOD1^{G93A}* Gene Induces Sarcolemma Damage

Previous studies (Barber et al., 2006; Mahoney et al., 2006) have found evidence of increased oxidative stress in ALS patients. Elevated levels of ROS can damage critical cellular components such as membrane lipids, structural and regulatory protein, and DNA (Moylan and Reid, 2007). We analyzed and compared the presence of oxidative damage in macromolecular substrates (lipids and proteins) in WT and in two different experimental transgenic models in which the function of cytosolic antioxidant enzyme SOD1 was affected: the SOD1^{G93A} transgenic mouse, which ubiquitously overexpresses mutant SOD1 (Gurney et al., 1994) and that represents the classical animal model of ALS, and the MLC/SOD1^{G93A} transgenic mouse described here. Malondialdehyde (MDA) (Figure 4A), a marker of lipid oxidative damage, was elevated in the sarcolemma of transgenic fibers of both SOD1^{G93A} and MLC/SOD1^{G93A} mice (Figure 4A). The membrane of the sarcoplasmic reticulum (SR) was significantly affected in SOD1^{G93A}, but not in MLC/SOD1^{G93A} transgenic muscle (Figure 4B). Additionally, the content of protein carbonyls, considered another marker of protein oxidative damage, increased in SOD1^{G93A} skeletal muscle but not in MLC/SOD1^{G93A}, compared to WT littermates (Figure 4C). These experiments suggest that alteration of SOD1 protein exclusively in skeletal muscle significantly damages the sarcolemma of muscle fibers, without affecting other targets altered by the ubiquitous expression of SOD1 mutant gene.

Muscle-Specific Expression of *SOD1^{G93A}* Mutant Gene Modulates Antioxidant Enzyme Activity

To explore the relationship between *SOD1^{G93A}* overexpression and signs of oxidative stress in skeletal muscle, we examined the main antioxidant enzyme activities, such as gluthathione reductase, gluthathione S-transferase, superoxide dismutase, and catalase, in muscles of both SOD1^{G93A} and MLC/SOD1^{G93A} mice. Notably, superoxide dismutase and catalase activity were significantly increased in both SOD1^{G93A} and MLC/SOD1^{G93A} muscles compared with WT mouse (Figure 4D). In addition, the classical SOD1^{G93A} transgenic mouse model displayed an increase in both glutathione S-transferase and glutathione reductase. In contrast, MLC/SOD1^{G93A} transgenic muscles did not demonstrate significant changes in glutathione S-transferase activity but rather a reduction in glutathione reductase activity compared with WT muscle. These experiments suggest that the SOD1^{G93A} mutation modulates redox-sensitive signaling cascades and antioxidant defense through distinct muscle-specific pathways.

To further prove that selective accumulation of ROS in skeletal muscle is causally linked to the induction of muscle atrophy and alteration in muscle strength observed in MLC/SOD1^{G93A} mice, we inhibited the accumulation of ROS and verified the potential prevention of SOD1^{G93A}-induced muscle abnormality.

To this purpose, MLC/SOD1^{G93A} mice were treated, intraperitoneally for 15 days, with 30 mg/Kg of Trolox, a cell-permeable water-soluble derivative of vitamin E with potent antioxidant properties (Wu et al., 1990; Salgo and Pryor, 1996). Notably, Trolox supplementation significantly reduced the toxic effect of ROS, rescuing muscle phenotype and the functional performance of transgenic muscle (Figures 4E and 4F).

Characterization of Molecular Pathways Involved in Oxidative Stress-Induced Muscle Atrophy

Transcriptional up- or downregulation of atrophy-related genes is a characteristic feature of muscle atrophy (Sandri et al., 2004). The most critical player of muscle atrophy is the transcription factor FoxO (Sandri et al., 2004). Western blot analysis revealed a selective accumulation of the dephosphorylated form of FoxO3 in MLC/SOD1^{G93A} transgenic muscles compared to WT mice (Figure 5A). The dephosphorylation/activation of FoxO3 would be expected to lead to upregulation of MAFbx/atrogin1 and MuRF1, which represent molecular targets of FoxO activity (Sandri et al., 2004). Surprisingly, quantitative reverse transcription polymerase chain reaction (RT-PCR) analysis revealed that while *MuRF1* expression increased in MLC/SOD1^{G93A} compared to WT mice (Figure 5B), *atrogin1* did not vary significantly between the two experimental models (Figure 5C), suggesting that FoxO-mediated atrogin1 expression can be partially repressed and/or other pathways may be involved in the ROS-mediated muscle atrophy. The first hypothesis is supported by the evidence that PGC1α, which increased in MLC/SOD1^{G93A} muscles (Figure 3H), inhibits FoxO-dependent transcription on atrogin1 promoter, thereby suppressing atrogin1 expression (Sandri et al., 2006).

More recently, it has been also reported that FoxO3 not only activates ubiquitin ligases but also is necessary and sufficient for the induction of autophagy, another important intracellular degradation mechanism, in skeletal muscle (Mammucari et al., 2007). This pathway is activated and operates under environmental stress conditions and in various pathological situations (Ohsumi, 2001). In line of this evidence we analyzed the potential downstream targets of FoxO3, including the autophagic markers cathepsin L, Bnip3, and LC3B. Cathepsin L is a lysosomal enzyme whose role appears to be the degradation of membrane proteins and that is known to be upregulated during skeletal muscle atrophy (Judge et al., 2007); Bnip3 is a Bcl-2-related BH3-only protein involved in the regulation of autophagy by inducing mitochondrial damage and removal via autophagosome (mitophagy) (Kubli et al., 2007); LC3 is an Atg8 homolog that is essential for autophagosome formation (Mammucari et al., 2007) and it is widely used to monitor autophagy.

Real-time RT-PCR analysis revealed that *cathepsin L*, *LC3*, and *Bnip3* were significantly upregulated in atrophic muscles of MLC/SOD1^{G93A} transgenic mice (Figures 5D–5F).

An alternative pathway that may be activated in ROS-mediated muscle atrophy is NFκB, a signaling pathway linked to

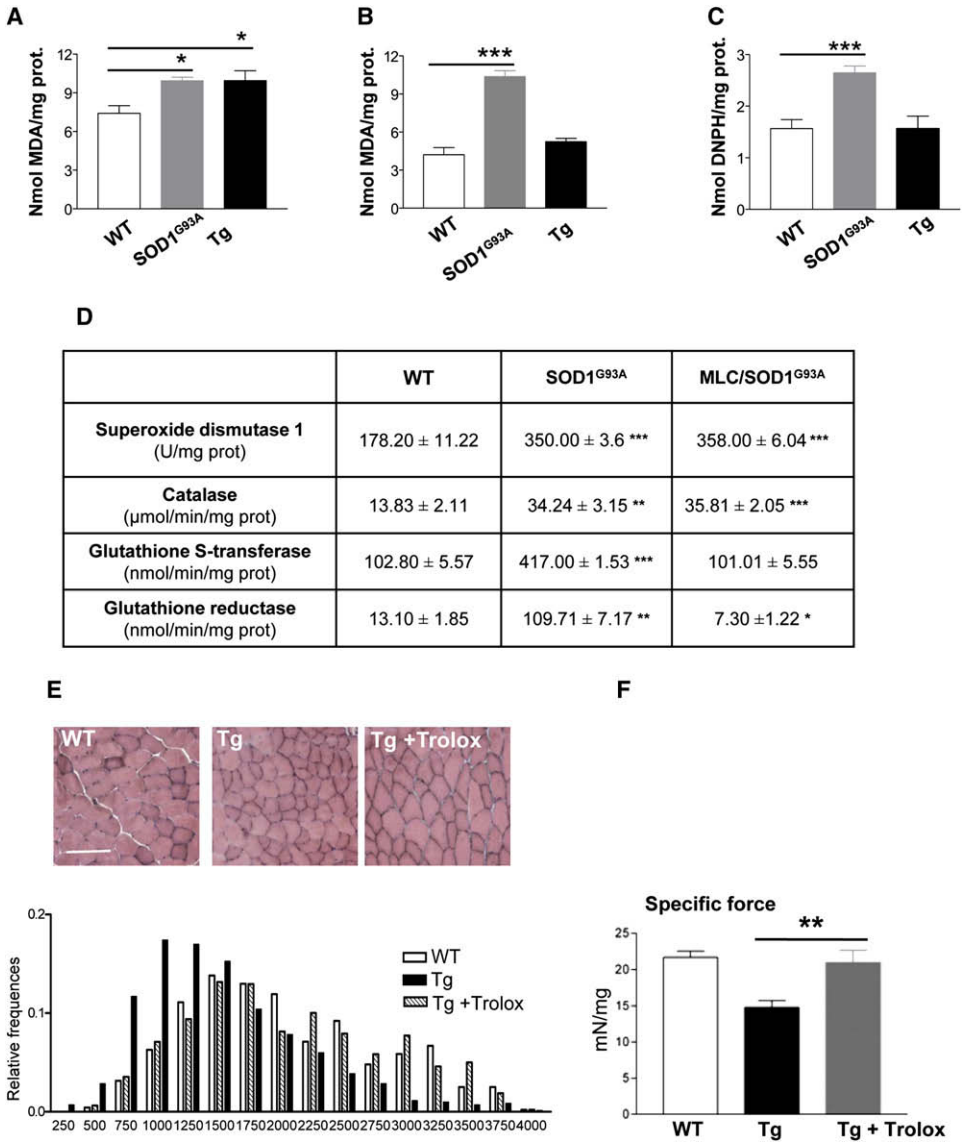

	WT	SOD1^{G93A}	MLC/SOD1^{G93A}
Superoxide dismutase 1 (U/mg prot)	178.20 ± 11.22	350.00 ± 3.6 ***	358.00 ± 6.04 ***
Catalase (μmol/min/mg prot)	13.83 ± 2.11	34.24 ± 3.15 **	35.81 ± 2.05 ***
Glutathione S-transferase (nmol/min/mg prot)	102.80 ± 5.57	417.00 ± 1.53 ***	101.01 ± 5.55
Glutathione reductase (nmol/min/mg prot)	13.10 ± 1.85	109.71 ± 7.17 **	7.30 ±1.22 *

Figure 4. Mutant SOD1^{G93A} Induces Oxidative Damage in Skeletal Muscle of Transgenic Mice

(A and B) Lipid peroxidation analysis, expressed as nmol of malondialdehyde (MDA) per mg of protein, in sarcolemma (A) and sarcoplasmic reticulum (B) membranes of wild-type (WT) (n = 5), SOD1^{G93A} (n = 5), and MLC/SOD1^{G93A} (Tg) (n = 5) mice. Values are mean ± SEM (*p < 0.05, ***p < 0.0001).

(C) Protein carbonyls assay from muscle of WT (n = 5), SOD1^{G93A} (n = 5), and MLC/SOD1^{G93A} (Tg) (n = 5) mice. The amounts of protein carbonyls are expressed as nmol of 2,4-dinitrophenylhydrazine (DNPH) per mg of protein. Values are mean ± SEM (*p < 0.05, ***p < 0.0001).

(D) Enzymatic activity of antioxidant enzymes superoxide dismutase 1, catalase, glutathione S-transferase, and glutathione reductase in skeletal muscle of WT (n = 5), SOD1^{G93A} (n = 5), and MLC/SOD1^{G93A} (Tg) (n = 5) mice. Data are expressed as mean ± SEM (*p < 0.05; **p < 0.0005; ***p < 0.0001).

(E) Top panel: Haematoxylin and eosin-stained cross-sections of TA muscles from WT and MLC/SOD1^{G93A} transgenic untreated (Tg) and treated with Trolox (Tg + Trolox) mice. Bar = 100 μm. Lower panel: Fiber size in WT (n = 6) and MLC/SOD1^{G93A} transgenic untreated (Tg) (n = 6) and treated (Tg + Trolox) mice of TA muscles (Mann-Whitney Rank Sum test: p < 0.0001).

(F) Specific force of EDL muscles from 4-month-old WT and transgenic untreated (Tg) and treated (Tg + Trolox) mice. All measurements are presented as mean ± SEM; **p < 0.002.

several pathologic processes in skeletal muscle (Bar-Shai et al., 2005). We analyzed this alternative pathway based on the interesting evidence that NFκB induces muscle atrophy and wasting, upregulating MuRF1 but not atrogin1 (Cai et al., 2004; Mourkioti et al., 2006), and based on the fact that a potential target of NFκB is cathepsin L (Judge et al., 2007), a lysosomal enzyme that we saw upregulated in atrophic muscle of MLC/SOD1^{G93A} mice (Figure 5D). Western blot analysis revealed an increase in the synthesis and in the phosphorylated form of NFκB protein (Figure 5G) in the atrophic muscles of MLC/SOD1^{G93A}, compared with WT mice, suggesting that the activation of both FoxO3 and NFκB converge on the autophagic pathway. Notably, in MLC/SOD1^{G93A} muscle we did not observe any significant modulation in apoptotic pathways, such as caspase, which are

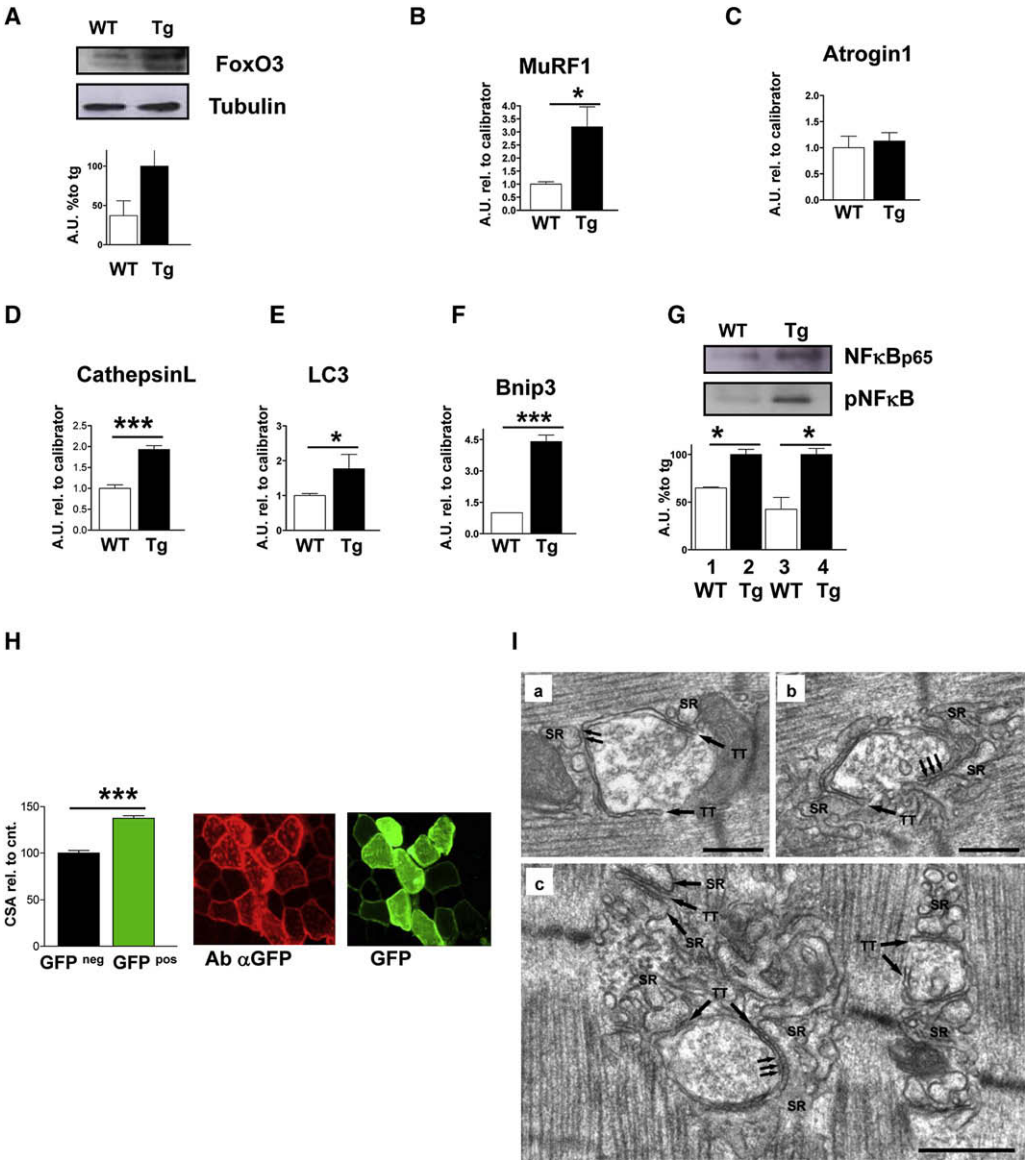

Figure 5. Molecular Signature of Muscle Atrophy Induced by MLC/SOD1^{G93A} Expression

(A) Upper panel: Representative western blot analysis of FoxO3 expression in EDL muscle of both wild-type (WT) and MLC/SOD1^{G93A} transgenic (Tg) mice. Lower panel shows densitometric analysis for FoxO expression.

(B–F) Real-time PCR for *MuRF1* (B), *atrogin1* (C), *cathepsin L* (D), *LC3* (E), and *Bnip3* (F) expression in both WT and MLC/SOD1^{G93A} (Tg) transgenic muscle (*$p = 0.03$; ***$p < 0.0001$).

(G) Upper panels show representative western blot analysis for NFκB and Phospho-NFκB expression in TA muscles of both WT and MLC/SOD1^{G93A} (Tg) mice. Lower panel shows densitometric analysis for NFκB (lanes 1 and 2) and Phospho-NFκB (lanes 3 and 4) expression (*$p < 0.05$).

(H) In vivo electrotransfer of siRNA-*LC3/GFP* construct in TA muscle of MLC/SOD1^{G93A} mice. Left panel shows the CSA of electroporated transgenic MLC/SOD1^{G93A} muscle.

Right panel shows a representative field of transfected (green–GFPpos and red–GFPpositive stained for anti-GFP antibody) and untransfected (dark–GFP-neg) fibers. The fibers that integrated the siRNA-LC3/GFP construct resulted in GFP-positive (GFPpos) and display rescue of atrophic phenotype when compared to wild-type fibers (data not shown). In contrast untransfected GFPneg fibers show the atrophic phenotype, compared with GFPpos fibers (***$p < 0.0001$). All values are mean ± SEM.

(I) Electron Microscopy of MLC/SOD1^{G93A} EDL muscles. Panels a–c show the altered interaction between sarcoplasmic reticulum (SR) and T-tubules. In MLC/SOD1^{G93A} muscles, SR and T-tubules were altered, with SR abnormally fragmented and the T-tubules forming a vacuole-like structure that encloses amorphous cytoplasmic material (a–c). Top left of panel c shows an area of muscle fibers in which SR and T-tubules are regularly organized in triads. Bars: a and c, 0.5 μm; b, 0.25 μm.

conversely activated in the classical animal model of ALS only at late stage of disease (Dobrowolny et al., 2008 and data not shown).

Taken together, these data suggest a feasible connection between SOD1^{G93A}-mediated oxidative stress and autophagy. To definitely prove the role of autophagy in the promotion of muscle

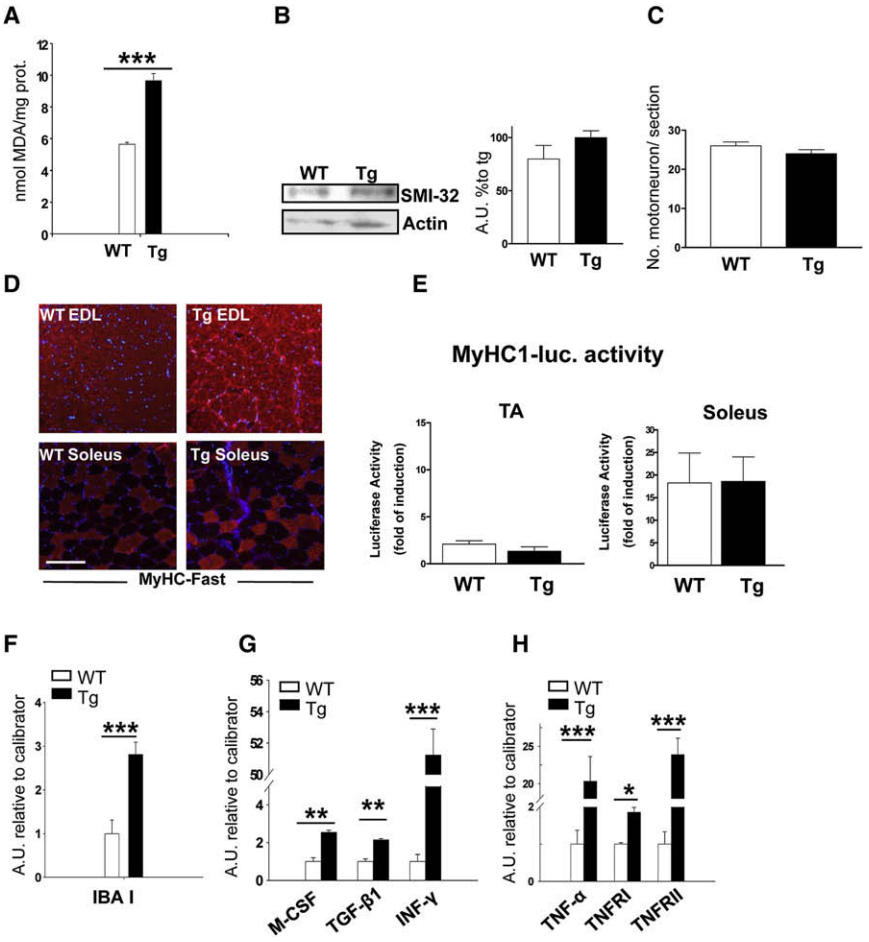

Figure 6. Muscle Expression of SOD1^{G93A} Mutant Gene Induces Presymptomatic Sign of ALS without Causing Motor Neuron Degeneration

(A) Lipid peroxidation, expressed as nmol of malondialdehyde (MDA) per mg of protein, in the spinal cord of wild-type (WT) (n = 5) and MLC/SOD1^{G93A} (Tg) (n = 5) mice. Values are mean ± SEM (*p < 0.0005).

(B) Representative western blot and densitometric analysis for SMI-32 expression in the ventral root of WT and MLC/SOD1^{G93A} (Tg) spinal cord.

(C) Quantification of surviving motor neurons in the ventral spinal cord of WT and MLC/SOD1^{G93A} (Tg) mice.

(D) Immunofluorescence analysis of transverse sections from soleus and EDL muscles of WT and MLC/SOD1^{G93A} (Tg) mice with antibodies against MyHC-Fast. Bar = 100 μm.

(E) Tibialis anterior (TA) and soleus muscles of 4-month-old mice (WT and Tg) were transfected with both Renilla pRL-TK construct and plasmid bearing a luciferase reporter driven by the MyHC1 promoter. Luciferase activity was measured in extracts from the muscles 1 week later.

(F–H) Real-time PCR of molecular markers of inflammatory response in the spinal cord of WT (white bars) (n = 5) and Tg (black bars) (n = 5) mice. Values are mean ± SEM (*p = 0.0146; **p < 0.005; ***p < 0.0001).

atrophy, we performed functional in vivo gene transfer experiments (Donà et al., 2003) into the TA (Figure 5H) and EDL (data not shown) myofibers of MLC/SOD1^{G93A} adult skeletal muscle. Using siRNA construct against *LC3* we demonstrated that the inactivation of *LC3* was sufficient to induce rescue of the muscle phenotype (Figure 5H).

One of the unresolved questions related to autophagy concerns the origin of the membrane that forms the sequestering vesicle. It has been proposed that autophagosomes might initiate from the modification of pre-existing structures (Wang and Klionsky, 2003). EM ultrastructural analysis of the sarcotubular system performed on MLC/SOD1^{G93A} fiber revealed significant alterations of internal (SR) and external (sarcolemma and transverse-tubules) membranes. SR in MLC/SOD1^{G93A} transgenic fibers was often abnormally fragmented (Figure 5I), and similar fragmented vesicles were also observed just below the sarcolemma (data not shown). These altered structures appear in proximity of areas in which disrupted mitochondria appear to be enveloped in membranous sacks (Figure 5Ia). In addition, an unexpected alteration in the transverse (T)-tubule organization was observed (Figure 5I). In WT muscle (data not shown), T-tubules run perpendicularly (transversely) to the long axis of the fiber and form junctions (or triads) with the SR terminal cisternae (Franzini-Armstrong, 1970). Notably, in MLC/SOD1^{G93A} mutant muscle, T-tubules curved into an L-like structure (Figure 5Ia) that progressed to a vesicle-like structure encompassing amorphous cellular material (Figures 5Ib and 5Ic). These structures were clearly of T-tubular origin since their association with the SR was still evident and RyR-feet were still present between the two membranes (Figures 5Ib and 5Ic, small arrows). Since ROS accumulation induced lipid peroxidation and sarcolemma damage (Figure 4A), it is reasonable to suggest that lipid peroxidation involves the entire plasma membrane, including T-tubules. Altered T-tubules (and possibly the SR) might be therefore the donor of membrane that forms the sequestering vesicles.

ROS Accumulation in Skeletal Muscle Inducing Microglia Activation without Motor Neuron Degeneration

One of the unresolved questions in ALS is whether muscle atrophy is directly induced by the toxic properties of muscle SOD1^{G93A} expression or whether it is a consequence of motor neuron degeneration. On the other hand, ROS-mediated muscle atrophy might retrogradely impact the nervous system and cause motor neuron loss. To verify this hypothesis, we analyzed specific targets of oxidative stress, such as lipid peroxidation, in the spinal cords of MLC/SOD1^{G93A} mice. MDA levels (Figure 6A) were elevated in the MLC/SOD1^{G93A} transgenic spinal cord compared to WT controls, indicating an alteration in the plasma membrane of motor neurons and suggesting that accumulated ROS in MLC/SOD1^{G93A} mutant muscle might influence and alter motor neuron activity. To verify this hypothesis, we performed

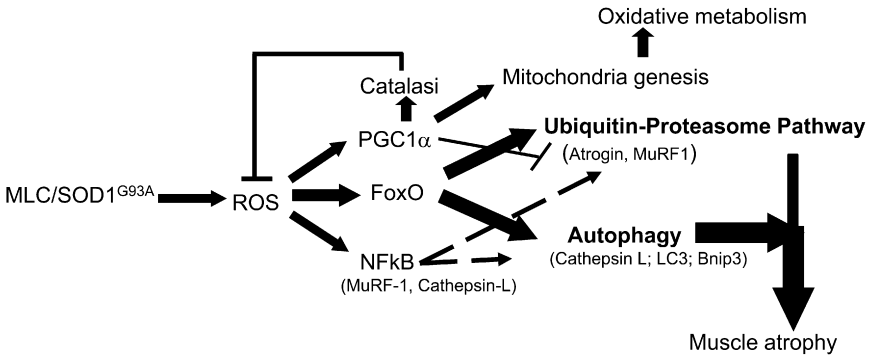

Figure 7. A Summary of the Role of the MLC/SOD1^{G93A} Transgene in the Modulation of Factors Involved in Muscle Atrophy
See text for details.

several experimental analyses, including motor neuron quantification in the ventral root of MLC/SOD1^{G93A} spinal cord.

Western blots (Figure 6B) and immunohistochemical analysis (Figure 6C) did not reveal significant changes in the number of motor neurons, rather pointing to a causal link between local accumulation of ROS and muscle atrophy. Other factors associated with muscle denervation and ALS severity are Nogo-A and Nogo-C (Jokic et al., 2006), whose expression, occurring early in ALS skeletal muscle, could cause repulsion and destabilization of the motor nerve terminals and subsequent dying back of the axons and motor neurons. Real-time RT-PCR analysis (data not shown) did not reveal significant change of *Nogo-A* and *Nogo-C* expression between WT and MLC/SOD1^{G93A} transgenic mice.

A shift in fiber composition constitutes another marker associated with muscle denervation (Schiaffino and Serrano, 2002). Specifically, motor neuron degeneration and muscle denervation cause a shift from slow to fast muscle phenotype. However, quantitative analysis of fiber composition in EDL and soleus muscles did not reveal significant differences between WT and MLC/SOD1^{G93A} transgenic adult mice (Figure 6D). This result was confirmed by analyzing the activity of slow-MyHC promoter (MyHC1-Luc) by in vivo functional electrotransfer (Figure 6E).

These data finally clarify that selective muscle accumulation of SOD1^{G93A} mutant protein does not induce motor neuron degeneration. Nevertheless, we analyzed in much detail whether and at which level the muscle accumulation of SOD1^{G93A} mutant protein and ROS impacts the nervous system. To this purpose we performed several experiments, based on the evidence that alteration in microglial activation and subsequent altered inflammatory response are associated with the presymptomatic sign of ALS and are independent from motor neuron degeneration (Neusch et al., 2007).

It has been recently reported that ROS can cross the motor neuron cell membrane and activate microglia, which respond by releasing cytokines and further ROS (Barber et al., 2006).

To characterize microglial responses in the MLC/SOD1^{G93A} mutant mice, we analyzed the expression of *ionized calcium-binding adaptor molecule* (*Iba1*), a specific marker of microglial cells (Imai et al., 1996). Quantitative RT-PCR analysis revealed a significant upregulation of *Iba1* expression in the spinal cord of MLC/SOD1^{G93A} transgenic mice, compared with WT littermates (Figure 6F). Notably, astrocyte activity, which normally increases at a later stage of ALS disease, did not change between WT and MLC/SOD1^{G93A} spinal cord, as revealed by GFAP expression (data not shown). The activation of microglia can be correlated with the expression of certain cytokines. In the spinal cord of the classical SOD1^{G93A} mouse model, *TGF-β1*, *M-CS*, *TNF-α*, and *TNF-α* receptor expression increases in young presymptomatic mice (Elliott, 2001). RT-PCR analysis (Figures 6G and 6H) revealed that *M-CSF*, *TGF-β1*, *INF-γ*, *TNF-α*, and *TNF-α* receptor expression accumulated in the spinal cord of MLC/SOD1^{G93A} mice, whereas their expression was maintained at low levels in the spinal cord of age-matched WT mice (Figures 6G and 6H).

Our data therefore suggest that additional pathways must be activated to trigger neuron degeneration and reinforce the evidence that skeletal muscle dysfunctions before motor neuron degeneration and the onset of clinical symptoms of ALS.

DISCUSSION

This study demonstrates that skeletal muscle is a direct target of SOD1 mutation and that muscle-restricted expression of *SOD1^{G93A}* gene is sufficient to induce severe muscle atrophy without evident sign of motor neuron degeneration. The original discovery of SOD1 gene mutations in ALS patients immediately prompted hypotheses of toxic gain-of-function effects on motor neurons. However, the pathogenesis of ALS is emerging as a "multisystemic" disease in which alterations in structural, physiological, and metabolic parameters in different cell types (motor neurons, glia, muscle) may act synergistically to exacerbate the disease, requiring a more directed approach to the analysis of aberrant SOD1 function in specific cell types. Although mutant SOD1 is also expressed by muscle of ALS patients the relative contribution of mutant *SOD1* gene expression in skeletal muscle has been debated (Miller et al., 2006).

Here we provide evidence for the local pathological impact of *SOD1* mutant gene (Figure 7). When overexpressed exclusively in skeletal muscle, mutant *SOD1^{G93A}* (1) induces accumulation of ROS and sarcolemma damage, (2) causes dramatic muscle atrophy with a concomitant alteration in the ultrastructure and in the functional performance of skeletal muscles, and (3) promotes a shift in the metabolic activity of muscle fibers.

The results of this study challenge the accepted dogma that motor neuron degeneration, caused by transgenic *SOD1^{G93A}* overexpression, is the primary cause of muscle atrophy.

Muscle atrophy represents one of the earliest events detectable in the SOD1^{G93A} ubiquitous transgenic animals (Brooks et al., 2004), followed by alteration of the neuromuscular junction, retrograde axonal degeneration, and lastly motor neuron death. This sequential pattern of degeneration suggests that certain muscle abnormalities precede motor neuron death rather than resulting from it. Our results confirm that local oxidative stress is a primary determinant of ALS-associated muscle

pathology, separating the toxic effects of *SOD1*^{G93A} transgene from motor neuron degeneration.

At first glance it would appear that the present study contradicts the work of Miller and coworkers (Miller et al., 2006), who reported that muscle is not a primary target for non-cell-autonomous toxicity in familial ALS. Their argument was based on the evidence that partial suppression of mutant protein accumulation within SOD1^{G93A} mouse muscle, using a lentivirus that encodes an siRNA directed against mutant SOD1, or by muscle selective *SOD1* mutant gene excision, did not delay the progression of the disease. Since we show that even low levels of local MLC/SOD1^{G93A} expression were sufficient to cause muscle atrophy and alteration in functional performance (Figures 2 and 3), both studies are consistent with the adverse effects of oxidative stress on muscle homeostasis.

How does oxidative stress induce muscle atrophy? Our experiments suggest that ROS production activates FoxO3, NFκB, and autophagic signaling (Figure 7). While FoxO3 modulates both *atrogin* and *MuRF1*, NFkB acts selectively on *MuRF1*. The action of FoxO is partly inhibited by PGC1α (Figure 7), a factor that is induced by oxidative stressors and that represents an important regulator of intracellular ROS levels. The activation of PGC1α also induces and coordinates gene expression that stimulates fiber-type switching and metabolic pathways, reflected in the increase in the number of mitochondria and therefore the shift from glycolytic to oxidative metabolism of MLC/SOD1^{G93A} transgenic muscle fibers.

It has also been reported that FoxO3 not only activates ubiquitin ligases but is also necessary and sufficient for the induction of the catabolic pathway known as autophagy (Figure 7) (Mammucari et al., 2007). The critical role of autophagy in the promotion of muscle atrophy was disclosed by genetic manipulation of *LC3* expression, suggesting that the modulation of autophagy can be a potential therapeutic intervention to counteract muscle atrophy associated with oxidative stress.

Although the mechanism whereby muscle contributes to ALS-associated motor neuron degeneration is still unclear, it is likely that toxic signals originating from skeletal muscle compromise the functional connection of muscle and nerve.

However, systemic interventions on several cell types are necessary to develop ALS disease and to trigger neuronal degeneration. Establishment of the myocyte as a direct target of the toxic properties of a mutant SOD1 variant provides important insights into the atrophic effects of oxidative stress in ALS disease.

EXPERIMENTAL PROCEDURES

Generation of MLC/SOD1^{G93A} Transgenic Mice

We subcloned both the *SOD1*^{G93A} and WT *SOD1* cDNAs into the pMex plasmid containing the regulatory elements of the MLC1f/3f gene (Figure 1A). FVB mice (Jackson Laboratories) were used as embryo donors. Positive founders were subsequently bred to FVB WT mice. Transgenic mice were selected by PCR using tail digests. The animals were housed in a temperature-controlled (22°C) room with a 12:12 hr light-dark cycle. All of the mice were maintained according to the institutional guidelines of the animal facilities of DIEM-National Institute of Health-Italy.

RNA Preparation and Northern Blot Analysis

We obtained total RNA from WT and MLC/SOD1^{G93A} transgenic muscles by TRIzol reagent (Invitrogen); 15 μg of RNA were fractionated by electrophoresis on 1.3% agarose gels and hybridized.

Protein Extraction and Western Blot Analysis

Protein extraction from both WT and MLC/SOD1^{G93A} transgenic muscles was performed in lysis buffer (50 mM Tris-HCl pH7.4, 1% w/v Triton x100, 0.25% sodium deoxycholate, 150 mM sodium chloride, 1 mM phenylmethylsulfonyl fluoride, 1 μg/ml aprotinin, 1 μg/ml leupeptin, 1 μg/ml pepstatin, 1 mM sodium orthovanadate, 1 mM sodium fluoride). Equal amounts of protein from each muscle lysate were separated in SDS polyacrilamide gel and transferred onto a nitrocellulose membrane. Filters were blotted with antibodies against human-SOD (BD Pharmigen), FoxO, NFκB, pNFκBSer 536 (Cell signaling), SMI-32 (AbCam), α-tubulin, and actin (Sigma).

Histological and Immunofluorescence Analysis

Segments of TA, EDL, and soleus muscles from WT and MLC/SOD1^{G93A} transgenic mice were embedded in tissue freezing medium and snap frozen in nitrogen-cooled isopentane and stained for either NADH-transferase or hematoxylin and eosin.

Additional muscle frozen sections (7 μm) were used for immunofluorescence analysis and processed as described in Dobrowolny and coworkers (2005). Monoclonal antibodies against myosin heavy chain (MyHC) I and II were used; nuclei were visualized using Hoechst staining.

For motor neuron quantification, fixed spinal cord slices were immunostained with SMI-32 monoclonal antibody. Inverted microscope (Axioskop 2 plus; Carl Zeiss MicroImaging, Inc.), using 20 or 40× lenses, was used and images were processed using Axiovision 3.1.

Morphometric Analysis and Statistics

A minimum of four random fields (corresponding to 400 cross-sectioned fibers) were photomicrographed for each muscle and mouse (n = 5/genotype); all type fibers were analyzed using Scion Image software (v. Beta 4.0.2, Scion, Frederick, MD). Statistical analysis was performed with GraphPad Prism v4.0 software; groups were compared by Mann-Whitney Rank Sum test and the difference in the median values between the two groups was considered significant for p value < 0.05.

Analysis of Oxidative Stress

Protein carbonyl content (Cayman Chemical) was measured by forming labeled protein hydrazone derivatives, using 2,4-dinitrophenylhydrazide (DNPH), and quantified spectrophotometrically (Mecocci et al., 1999). Results are expressed as nmol of DNPH per mg of proteins. MDA dosage was performed by means of a HPLC system with fluorometric detection (Mecocci et al., 1999). MDA forms an adduct with thiobarbituric acid (TBA) that is measured by spectrophotometry (OXItek TBARS Assay Kit; ZeptoMetrix Corporation). Results are expressed as nmol of MDA per mg of proteins.

Antioxidant Enzymes Activities

The antioxidant enzyme assays were performed, as previously detailed (Fanò et al., 2001). Muscle tissue was homogenized in ten volumes of 20 mM Na-phosphate buffer pH 7.0 + 1 μg/ml pepstatin, 1 μg/ml leupeptin, and 100 μM phenylmethylsulfonyl fluoride (PMSF) as protease inhibitors and centrifuged at 100,000 × g for 1 hr at 4°C. Cytosol proteins were measured on the resulting supernatant according to the Lowry's method. Superoxide dismutase (SOD) activity was determined using the modified method by Fulle and coworkers (Fulle et al., 2000). Catalase (Cat) activity was determined, analyzing the decrease in absorbance due to H_2O_2 consumption ($\varepsilon = -0.04$ mM-1 cm-1) measured at 240 nm. The final reaction volume was 1 ml and contained 100 mM Na-phosphate buffer pH 7.0, 12 μM H_2O_2, and 70 μg of protein lysate. Glutathione S-transferase (GSt) activity was determined by using 1-cloro-2-4-dinitrobenzene (CDNB) as substrate. The assay was performed at 340 nm (ε = 9.6 mM-1 cm-1) in a final volume of 1 ml containing 100 mM Na-phosphate buffer pH 6.5, 1 mM CDNB, 1 mM reduced glutathione (GSH), and 30 μg of protein lysate. Glutathione reductase (GR) activity was measured by the rate of decrease in absorbance, induced by NADPH oxidation, at 340 nm ($\varepsilon = -6.22$ mM-1 cm-1). The assay mixture contained, in a final volume of 1 ml, 100 mM Na-phosphate buffer pH 7.0, 1 mM glutathione disulphide (GSSG), 60 μM NADPH, and 100 μg of protein lysate.

Trolox Treatment

MLC/SOD1^{G93A} transgenic mice (n = 6) were treated daily for 15 days with 30 mg/kg of Trolox intraperitoneally.

Mechanical Measurements

EDL and soleus muscles were isolated from 4-month-old WT and transgenic mice and transferred to a dissecting chamber, containing Krebs-Ringer solution at room temperature (RT) equilibrated with 5% CO_2-95% O_2 (pH 7.30). The proximal tendon was fixed to a clamp and the distal tendon to a force transducer (model Aurora Scientific Instruments 300B).

The isolated muscle was electrically stimulated by means of two platinum electrodes, located 2 mm from each side of the muscle, with 200 mA controlled current pulses (Del Prete et al., 2008). Optimum muscle length was adjusted to the length (L_o) that produced the highest twitch force. Maximum tetanic force was measured with a train of pulses delivered at 180 Hz for EDL and 60 Hz for soleus. Specific force was computed as maximum force divided by muscle weight. To evaluate mechanical work the muscle was repeatedly stimulated in isotonic conditions with a series of 0.1 ms pulses (120 Hz for EDL and 60 Hz for soleus), delivered in trains of 0.4 s duration, repeated every 1 s (Del Prete et al., 2008). In this phase the muscle shortened against a load equal to one-third of its own maximum force. This value was chosen because it has been shown that unfatigued muscles generate their maximum power at that force level (Vedsted et al., 2003). Mechanical work was calculated by multiplying the constant load with the displacement measured during each contraction.

RNAi and Adult Mouse Skeletal Muscle Transfection

In vivo RNAi experiments were performed as previously described (Sandri et al., 2004), using the sequence (actctgatgcactaataaa) that targets regions in the mouse *LC3* gene, and RNAi was cloned into pSUPER vector bearing the GFP reporter gene; mice were sacrificed 7 and 21 days after transfection. CSA of GFP-positive and GFP-negative fibers were measured as described in Morphometric Analysis and Statistics section.

Electron Microscopy

EDL and TA muscles were carefully dissected from transgenic and WT mice (4 months of age). Muscles were fixed immediately at RT in 3.5% glutaraldehyde in 0.1 M Na cacodylate buffer, pH 7.2, for 2 hr. Small bundles of fixed fibers were then post-fixed in 2% OsO4 in the same buffer for 2 hr and block-stained in aqueous saturated uranyl acetate. Ultra thin sections were cut in a Leica Ultracut R microtome (Leica Microsystem, Vienna, Austria) using a Diatome diamond knife (DiatomeLtd. CH-2501 Biel, Switzerland). Sections, after staining in 4% uranyl acetate and lead citrate, were examined with a Morgagni Series 268D electron microscope (FEI Company, Brno, Czech Republic), equipped with Megaview III digital camera.

RNA Extraction and Quantitative RT-PCR

Total RNA (1 μg) was treated with DNase I Amplification Grade (Invitrogen) and reverse-transcribed using the SuperScript III (Invitrogen). Quantitative PCR was performed using the ABI PRISM 7000 SDS (Applied Biosystems, USA), and iTaqSupermix with rox (Biorad). All primers were optimized for real-time RT-PCR amplification, checking the generation of a single amplicon in a melting curve assay and the efficiency in a standard curve amplification (>98% for each couple of primers). Quantitative RT-PCR sample value was normalized for the expression of 18 s mRNA. The relative level for each gene was calculated using the $2^{-\Delta\Delta Ct}$ method (Livak and Schmittgen, 2001) and reported as arbitrary units.

Sequences of Primers Used in Quantitative Real-Time PCR

PGC1α: 5′ggaatgcaccgtaaatctgc3′ 5′ttctcaagagcagcgaaagc3′;
Murf-1: 5′acctgctggtggaaaacatc3′ 5′cttcgtgttccttgcacatc3′;
Atrogin1: 5′gcaaacactgccacattctctc3′ 5′cttgaggggaaagtgagacg3′;
Bnip3: 5′ttccactagcaccttctgatga3′ 5′gaacaccgcatttacagaacaa3′;
LC3: 5′cactgctctgtcttgtgtaggttg3′ 5′tcgttgtgcctttattagtgcatc3′;
Cathepsin L: 5′gtggactgttctcacgctcaag3′ 5′tccgtccttcgcttcatagg3′.

Statistical Analysis

All data, if not differently specified, were compared using Student's t test, with $p < 0.05$ being considered statistically significant.

ACKNOWLEDGMENTS

We thank M.T. Carrì for reagents; T. Rando, B.M. Scicchitano, and D. Sassoon for critical comments on this manuscript; and J. Gonzales and E. Magnani for technical support. This work was supported by MDA and Telethon (GGP06004) and partly by AFM, AIRC, MIUR, and ASI to A.M. and in part by Sport Medicine and Telethon to F.P.; by ASI, Telethon, AFM, and Compagnia San Paolo to M.S.; and by MATT and University G. d'Annunzio Foundation to G.F.

Received: May 16, 2008
Revised: August 4, 2008
Accepted: September 9, 2008
Published: November 4, 2008

REFERENCES

Barber, S.C., Mead, R.J., and Shaw, P.J. (2006). Oxidative stress in ALS: a mechanism of neurodegeneration and a therapeutic target. Biochim. Biophys. Acta *1762*, 1051–1067.

Bar-Shai, M., Carmeli, E., and Reznick, A.Z. (2005). The role of NF-kappaB in protein breakdown in immobilization, aging, and exercise: from basic processes to promotion of health. Ann. N Y Acad. Sci. *1057*, 431–447.

Boncompagni, S., d'Amelio, L., Fulle, S., Fanò, G., and Protasi, F. (2006). Progressive disorganization of the excitation-contraction coupling apparatus in aging human skeletal muscle as revealed by electron microscopy: a possible role in the decline of muscle performance. J. Gerontol. A Biol. Sci. Med. Sci. *61*, 995–1008.

Brooks, K.J., Hill, M.D., Hockings, P.D., and Reid, D.G. (2004). MRI detects early hindlimb muscle atrophy in Gly93Ala superoxide dismutase-1 (G93A SOD1) transgenic mice, an animal model of familial amyotrophic lateral sclerosis. NMR Biomed. *17*, 28–32.

Cai, D., Frantz, J.D., Tawa, N.E., Melendez, P.A., Oh, B.C., Lidov, H.G., Hasselgren, P.O., Frontera, W.R., Lee, J., Glass, D.J., et al. (2004). IKKbeta/NF-kappaB activation causes severe muscle wasting in mice. Cell *119*, 285–298.

Chung, M.J., and Suh, Y.L. (2002). Ultrastructural changes of mitochondria in the skeletal muscle of patients with amyotrophic lateral sclerosis. Ultrastruct. Pathol. *26*, 3–7.

Del Prete, Z., Musarò, A., and Rizzuto, E. (2008). Measuring mechanical properties, including isotonic fatigue, of fast and slow MLC/mIgf-1 transgenic skeletal muscle. Ann. Biomed. Eng. *36*, 1281–1290.

Dobrowolny, G., Giacinti, C., Pelosi, L., Nicoletti, C., Winn, N., Barberi, L., Molinaro, M., Rosenthal, N., and Musarò, A. (2005). Muscle expression of a local Igf-1 isoform protects motor neurons in an ALS mouse model. J. Cell Biol. *168*, 193–199.

Dobrowolny, G., Aucello, M., Molinaro, M., and Musarò, A. (2008). Local expression of mIgf-1 modulates ubiquitin, caspase and CDK5 expression in skeletal muscle of an ALS mouse model. Neurol. Res. *30*, 131–136.

Donà, M., Sandri, M., Rossini, K., Dell'Aica, I., Podhorska-Okolow, M., and Carraro, U. (2003). Functional in vivo gene transfer into the myofibers of adult skeletal muscle. Biochem. Biophys. Res. Commun. *312*, 1132–1138.

Elliott, J.L. (2001). Cytokine upregulation in a murine model of familial amyotrophic lateral sclerosis. Brain Res. Mol. Brain Res. *95*, 172–178.

Fanò, G., Mecocci, P., Vecchiet, J., Belia, S., Fulle, S., Polidori, M.C., Felzani, G., Senin, U., Vecchiet, L., and Beal, M.F. (2001). Age and sex influence on oxidative damage and functional status in human skeletal muscle. J. Muscle Res. Cell Motil. *22*, 345–351.

Franzini-Armstrong, C. (1970). Studies of the triad. J. Cell Biol. *47*, 488–499.

Fulle, S., Mecocci, P., Fano, G., Vecchiet, I., Vecchini, A., Racciotti, D., Cherubini, A., Pizzigallo, E., Vecchiet, L., Senin, U., et al. (2000). Specific oxidative alterations in vastus lateralis muscle of patients with the diagnosis of chronic fatigue syndrome. Free Radic. Biol. Med. *29*, 1252–1259.

Grieshammer, U., Sassoon, D., and Rosenthal, N.A. (1992). Transgene target for positional regulators marks early rostrocaudal specification of myogenic lineages. Cell *69*, 79–93.

Gurney, M.E., Pu, H., Chiu, A.Y., Dal Canto, M.C., Polchow, C.Y., Alexander, D.D., Caliendo, J., Hentati, A., Kwon, Y.W., Deng, H.X., et al. (1994). Motor neuron degeneration in mice that express a human Cu,Zn superoxide dismutase mutation. Science *264*, 1772–1775.

Imai, Y., Ibata, I., Ito, D., Ohsawa, K., and Kohsaka, S. (1996). A novel gene iba1 in the major histocompatibility complex class III region encoding an EF hand protein expressed in a monocytic lineage. Biochem. Biophys. Res. Commun. *224*, 855–862.

Jokic, N., Gonzalez de Aguilar, J.L., Dimou, L., Lin, S., Fergani, A., Ruegg, M.A., Schwab, M.E., Dupuis, L., and Loeffler, J.P. (2006). The neurite outgrowth inhibitor Nogo-A promotes denervation in an amyotrophic lateral sclerosis model. EMBO Rep. *7*, 1162–1167.

Judge, A.R., Koncarevic, A., Hunter, R.B., Liou, H.C., Jackman, R.W., and Kandarian, S.C. (2007). Role for IkappaBalpha, but not c-Rel, in skeletal muscle atrophy. Am. J. Physiol. Cell Physiol. *292*, 372–382.

Kubli, D.A., Ycaza, J.E., and Gustafsson, A.B. (2007). Bnip3 mediates mitochondrial dysfunction and cell death through Bax and Bak. Biochem. J. *405*, 407–415.

Lin, J., Wu, H., Tarr, P.T., Zhang, C.Y., Wu, Z., Boss, O., Michael, L.F., Puigserver, P., Isotani, E., Olson, E.N., et al. (2002). Transcriptional co-activator PGC-1 alpha drives the formation of slow-twitch muscle fibres. Nature *418*, 797–801.

Livak, K.J., and Schmittgen, T.D. (2001). Analysis of relative gene expression data using real-time quantitative PCR and the $2^{-\Delta\Delta Ct}$ method. Methods *25*, 402–408.

Mahoney, D.J., Kaczor, J.J., Bourgeois, J., Yasuda, N., and Tarnopolsky, M.A. (2006). Oxidative stress and antioxidant enzyme upregulation in SOD1–G93A mouse skeletal muscle. Muscle Nerve *33*, 809–816.

Mammucari, C., Milan, G., Romanello, V., Masiero, E., Rudolf, R., Del Piccolo, P., Burden, S.J., Di Lisi, R., Sandri, C., Zhao, J., et al. (2007). FoxO3 controls autophagy in skeletal muscle in vivo. Cell Metab. *6*, 458–471.

Mecocci, P., Fano, G., Fulle, S., MacGarvey, U., Shinobu, L., Polidori, M.C., Cherubini, A., Vecchiet, J., Senin, U., and Beal, M.F. (1999). Age-dependent increases in oxidative damage to DNA, lipids, and proteins in human skeletal muscle. Free Radic. Biol. Med. *26*, 303–308.

Miller, T.M., Kim, S.H., Yamanaka, K., Hester, M., Umapathi, P., Arnson, H., Rizo, L., Mendell, J.R., Gage, F.H., Cleveland, D.W., and Kaspar, B.K. (2006). Gene transfer demonstrates that muscle is not a primary target for non-cell-autonomous toxicity in familial amyotrophic lateral sclerosis. Proc. Natl. Acad. Sci. USA *103*, 19546–19551.

Mourkioti, F., Kratsios, P., Luedde, T., Song, Y.H., Delafontaine, P., Adami, R., Parente, V., Bottinelli, R., Pasparakis, M., and Rosenthal, N. (2006). Targeted ablation of IKK2 improves skeletal muscle strength, maintains mass, and promotes regeneration. J. Clin. Invest. *116*, 2945–2954.

Moylan, J.S., and Reid, M.B. (2007). Oxidative stress, chronic disease, and muscle wasting. Muscle Nerve *4*, 411–429.

Neusch, C., Bähr, M., and Schneider-Gold, C. (2007). Glia cells in amyotrophic lateral sclerosis: new clues to understanding an old disease? Muscle Nerve *35*, 712–724.

Ogata, T., and Yamasaki, Y. (1985). Scanning electron-microscopic studies on the three-dimensional structure of mitochondria in the mammalian red, white and intermediate muscle fibers. Cell Tissue Res. *241*, 251–256.

Ohsumi, Y. (2001). Molecular dissection of autophagy: two ubiquitin-like systems. Nat. Rev. Mol. Cell Biol. *3*, 211–216.

Salgo, M.G., and Pryor, W.A. (1996). Trolox inhibits peroxynitrite-mediated oxidative stress and apoptosis in rat thymocytes. Arch. Biochem. Biophys. *333*, 482–488.

Sandri, M., Sandri, C., Gilbert, A., Skurk, C., Calabria, E., Picard, A., Walsh, K., Schiaffino, S., Lecker, S.H., and Goldberg, A.L. (2004). Foxo transcription factors induce the atrophy-related ubiquitin ligase atrogin-1 and cause skeletal muscle atrophy. Cell *117*, 399–412.

Sandri, M., Lin, J., Handschin, C., Yang, W., Arany, Z.P., Lecker, S.H., Goldberg, A.L., and Spiegelman, B.M. (2006). PGC-1alpha protects skeletal muscle from atrophy by suppressing FoxO3 action and atrophy-specific gene transcription. Proc. Natl. Acad. Sci. USA *103*, 16260–16265.

Schiaffino, S., and Serrano, A. (2002). Calcineurin signaling and neural control of skeletal muscle fiber type and size. Trends Pharmacol. Sci. *23*, 569–575.

St-Pierre, J., Drori, S., Uldry, M., Silvaggi, J.M., Rhee, J., Jäger, S., Handschin, C., Zheng, K., Lin, J., Yang, W., et al. (2006). Suppression of reactive oxygen species and neurodegeneration by the PGC-1 transcriptional coactivators. Cell *127*, 397–408.

Vedsted, P., Larsen, A.H., Madsen, K., and Sjogaard, G. (2003). Muscle performance following fatigue induced by isotonic and quasi-isometric contractions of rat extensor digitorum longus and soleus muscles in vitro. Acta Physiol. Scand. *178*, 175–186.

Wang, C.W., and Klionsky, D.J. (2003). The molecular mechanism of autophagy. Mol. Med. *9*, 65–76.

Wu, T.W., Hashimoto, N., Wu, J., Carey, D., Li, R.K., Mickle, D.A., and Weisel, R.D. (1990). The cytoprotective effect of Trolox demonstrated with three types of human cells. Biochem. Cell Biol. *68*, 1189–1194.